Lithographically and electrically controlled strain effects on anisotropic magnetoresistance in (Ga,Mn)As

E De Ranieri[1,2,5]**, A W Rushforth**[3]**, K Výborný**[4]**, U Rana**[1,2]**,
E Ahmad**[3]**, R P Campion**[3]**, C T Foxon**[3]**, B L Gallagher**[3]**,
A C Irvine**[1] **and T Jungwirth**[3,4]

[1] Microelectronics Research Centre, Cavendish Laboratory,
University of Cambridge, Cambridge CB3 0HE, UK
[2] Hitachi Cambridge Laboratory, Cambridge CB3 0HE, UK
[3] School of Physics and Astronomy, University of Nottingham,
Nottingham NG7 2RD, UK
[4] Institute of Physics ASCR, v.v.i., Cukrovarnická 10, 162 53 Praha 6,
Czech Republic
E-mail: ed299@cam.ac.uk

Abstract. It has been demonstrated that magnetocrystalline anisotropies in (Ga,Mn)As are sensitive to lattice strains as small as 10^{-4} and that strain can be controlled by lattice parameter engineering during growth, through post-growth lithography, and electrically by bonding the (Ga,Mn)As sample to a piezoelectric transducer (PZT). In this work, we show that analogous effects are observed in crystalline components of the anisotropic magnetoresistance (AMR). Lithographically or electrically induced strain variations can produce crystalline AMR components which are larger than the crystalline AMR and a significant fraction of the total AMR of the unprocessed (Ga,Mn)As material. In these experiments, we also observe new higher order terms in the phenomenological AMR expressions which were previously unnoticed in (Ga,Mn)As. It is demonstrated that strain variation effects can play an important role in the magnetotransport characteristics of (Ga,Mn)As lateral nanoconstrictions.

[5] Author to whom any correspondence should be addressed.

IOP Institute of Physics ⊕ DEUTSCHE PHYSIKALISCHE GESELLSCHAFT

Contents

1. Introduction

GaAs doped with ∼1–10% of the magnetic acceptor Mn is a unique material for exploring spin–orbit coupling effects on micromagnetic and magnetotransport characteristics of ferromagnetic spintronic devices. Spin-polarized valence band holes that mediate ferromagnetic coupling between Mn local moments, produce large magnetic stiffness, resulting in a mean field-like magnetization and macroscopic single-domain behavior of these dilute moment ferromagnets. At the same time, magnetocrystalline anisotropies derived from spin–orbit coupling effects in the hole valence bands are large, leading to the sensitivity of the magnetic state to strains as small as 10^{-4} [1]–[5]. Experimentally, strain effects can be controlled by lattice parameter engineering during growth [6, 7] and through post-growth lithography [1]–[3]. Electrical control is achieved by bonding a piezoelectric transducer (PZT), e.g. the lead zirconate titanate, to the (Ga,Mn)As sample [4, 5, 8], in analogy with previous experiments in metal ferromagnets [9]–[12]. Easy axis rotations from the in-plane to out-of-plane directions have been demonstrated in these studies in (Ga,Mn)As films grown under compressive and tensile lattice matching strains, and the orientation of the in-plane easy axis (axes) has been shown to respond to strain relaxation in lateral microstructures or controlled electrically by the piezo-stressors.

Strain control of magnetocrystalline effects on transport in (Ga,Mn)As, which we focus on in this paper, has so far been explored less extensively. It has been reported that symmetries lowered by the growth lattice-mismatch strain [13]–[15] or on high-index surfaces [16] induce additional anisotropic magneto resistance (AMR) contributions in (Ga,Mn)As, similar to other magnetic materials [17, 18]. These theoretical and experimental studies have shown that the magnetotransport coefficients can be large and reflect the rich magnetocrystalline anisotropies of the studied (Ga,Mn)As materials [13, 15, 16], [19]–[24].

In this paper, we demonstrate that the post-growth strain manipulation procedures can also significantly change the AMR in (Ga,Mn)As. We report and analyze AMR measurements in strain-relaxed (Ga,Mn)As micro and nanostructures, and in a (Ga,Mn)As film bonded to a PZT. The resulting lattice distortions strongly modify crystalline AMR terms and give rise to new, previously undetected components in phenomenological AMR expansions applied to (Ga,Mn)As. The methods to control AMR after growth described here are much more flexible than the growth techniques used previously. They allow for a continuous tuning of the strain

effects on AMR with all other material parameters fixed and, therefore, a very systematic exploration of the AMR phenomenology and microscopic origins in (Ga,Mn)As.

The present paper is organized as follows: an extension of the phenomenological symmetry analysis of Döring [25] is given in section 2 with details of the derivation described in appendix A. Our goal was to organize the definitions of the transport anisotropy constants in a way that would facilitate straightforward comparisons between the experimental data and microscopic theories. In appendix B, we comment on the relation between our notation and several other notations which have appeared in the literature. Lithographical engineering of *transport* anisotropies due to the relaxation of the lattice-mismatch strain is reported in section 3 for (Ga,Mn)As micro Hall-bars and nanoconstriction device. In section 4, we discuss the other approach to post-growth strain manipulation exploiting hybrid PZT/(Ga,Mn)As structures.

2. Phenomenological description of the AMR

We consider a thin film geometry and a magnetization vector, $\vec{M}/|\vec{M}| = (\cos \psi, \sin \psi)$, in the plane of the film with its two components defined with respect to the orthogonal crystallographic basis {[100], [010]}. The resistivity tensor,

$$\hat{\rho} = \begin{pmatrix} \rho_{11}(\cos \psi, \sin \psi) & \rho_{12}(\cos \psi, \sin \psi) \\ \rho_{21}(\cos \psi, \sin \psi) & \rho_{22}(\cos \psi, \sin \psi) \end{pmatrix}, \tag{1}$$

written in the same basis describes the longitudinal and transverse resistivities of a pair of Hall bar devices oriented along the [100]-direction (ρ_{11} and ρ_{21}) and the [010]-direction (ρ_{22} and ρ_{12}). Resistivities of a pair of orthogonal Hall bars tilted by an angle θ from the [100]/[010] directions are given by $R_{-\theta}\hat{\rho}R_{\theta}$, where

$$R_{\theta} = \begin{pmatrix} \cos \theta & -\sin \theta \\ \sin \theta & \cos \theta \end{pmatrix}$$

is the rotation matrix. Written explicitly, the longitudinal (ρ_{L}) and transverse (ρ_{T}) resistivities for the Hall bar rotated by the angle θ from the [100]-direction read

$$\rho_{\mathrm{L}} = (\cos \theta, \sin \theta)\, \hat{\rho} \begin{pmatrix} \cos \theta \\ \sin \theta \end{pmatrix},$$

$$\rho_{\mathrm{T}} = (\cos \theta, \sin \theta)\, \hat{\rho} \begin{pmatrix} -\sin \theta \\ \cos \theta \end{pmatrix}. \tag{2}$$

We first derive expressions for the non-crystalline AMR components [23, 26] which depend only on the angle $\psi - \theta$ between the current (Hall bar orientation) and the magnetization vector, and which account for the AMR in isotropic (polycrystalline) materials. We expand the elements of $\hat{\rho}$ in equation (1) in series of $\cos^n \psi$ and $\sin^n \psi$ [25], or equivalently of $\cos n\psi$ and $\sin n\psi$. The form of equation (2) implies that corresponding expansions of ρ_{L} and ρ_{T} in series of $\cos(n\psi + m\theta)$ and $\sin(n\psi + m\theta)$ contain only terms with $m = 0, \pm 2$. Among those, the $\cos 2(\psi - \theta)$ and $\sin 2(\psi - \theta)$ are the only terms depending solely on $\psi - \theta$. This explains why the non-crystalline AMR components, which are obtained by truncating equation (1) to

$$\hat{\rho} = \rho_{\mathrm{av}} \begin{pmatrix} 1 & 0 \\ 0 & 1 \end{pmatrix} + 2\rho_{\mathrm{av}} C_I \begin{pmatrix} -\frac{1}{2} + \cos^2 \psi & \sin \psi \cos \psi \\ \sin \psi \cos \psi & -\frac{1}{2} + \sin^2 \psi \end{pmatrix}, \tag{3}$$

take the simple form $\Delta\rho_L/\rho_{av} \equiv (\rho_L - \rho_{av})/\rho_{av} = C_I \cos 2(\psi - \theta)$ and $\rho_T/\rho_{av} = C_I \sin 2(\psi - \theta)$ [23, 26]. Here ρ_{av} is the average (with respect to ψ) longitudinal resistivity, and C_I is the non-crystalline AMR amplitude.

All terms in the expansion of equation (2) which depend explicitly on the orientation of the magnetization vector with respect to the crystallographic axes contribute to the crystalline AMR [23, 26]. Symmetry considerations can be used to find the form of $\hat{\rho}(\psi)$ in equation (1) specific to a particular crystal structure. Explicit expressions for $\hat{\rho}(\psi)$ in unperturbed cubic crystals, and cubic crystals with uniaxial strains along the [110]- and [100]-axes are derived in appendix A. Here, we write the final expression for ρ_L and ρ_T obtained from the particular form of $\hat{\rho}(\psi)$ and from equation (2). For the cubic lattice, omitting terms with the periodicity in ψ smaller than 90°, we obtain,

$$\frac{\Delta\rho_L}{\rho_{av}} = C_I \cos 2(\psi - \theta) + C_{IC} \cos(2\psi + 2\theta) + C_C \cos 4\psi + \cdots \tag{4}$$

$$\frac{\rho_T}{\rho_{av}} = C_I \sin 2(\psi - \theta) - C_{IC} \sin(2\psi + 2\theta) + \cdots. \tag{5}$$

For the higher order cubic terms, see appendix A. Some terms in this expansion coincide with or are contained in results presented in earlier works [16, 25, 26] (as explained in appendix B). While we understand that the reader may be overwhelmed with the various definitions of anisotropy constants, we stress that the previous definitions are based on power expansions in terms of $\cos^n \psi$ in equation (1). This leads to inconvenient expressions, given that experimental data are usually analyzed in terms of $\cos n\psi$. Advantages of the present notation are highlighted in appendix B.

Additional components emerge in $\Delta\rho_L/\rho_{av}$ and ρ_T/ρ_{av} for the uniaxially strained lattice which we denote as Δ_L^{uni} and Δ_T^{uni}, respectively. Omitting terms with the periodicity in ψ smaller than 180° we obtain,

$$
\begin{aligned}
(\pm)\Delta_L^{uni} &= C_{IU}^s \sin 2\theta + C_U^s \sin 2\psi, \\
(\pm)\Delta_T^{uni} &= C_{IU}^s \cos 2\theta
\end{aligned}
\tag{6}
$$

for strain along the in-plane diagonal directions ($s = [110]$ corresponds to '+' and $[1\bar{1}0]$ to '−'), and

$$
\begin{aligned}
(\pm)\Delta_L^{uni} &= C_{IU}^s \cos 2\theta + C_U^s \cos 2\psi, \\
(\pm)\Delta_T^{uni} &= -C_{IU}^s \sin 2\theta + C_{U,T}^s \sin 2\psi
\end{aligned}
\tag{7}
$$

for strain along the in-plane cube edges ($s = [100]$ corresponds to '+' and [010] to '−'). For higher order uniaxial terms see again appendix A.

3. Experiments in lithographically patterned (Ga,Mn)As microdevices

We now proceed with the discussion of AMR measurements in (Ga,Mn)As microdevices in which strain effects are controlled by lithographically induced lattice relaxation [1]–[3]. A sketch of the first studied device is shown in figure 1(a). The structure consists of four $1 \, \mu$m wide Hall bars and one $40 \, \mu$m wide bar connected in series. The wider bar is aligned along the [010]-crystallographic direction, the microbars are oriented along the [110]-, [1$\bar{1}$0]-, [100]- and [010]-axes. The Hall bars are defined by $500 \, $nm wide trenches patterned by e-beam
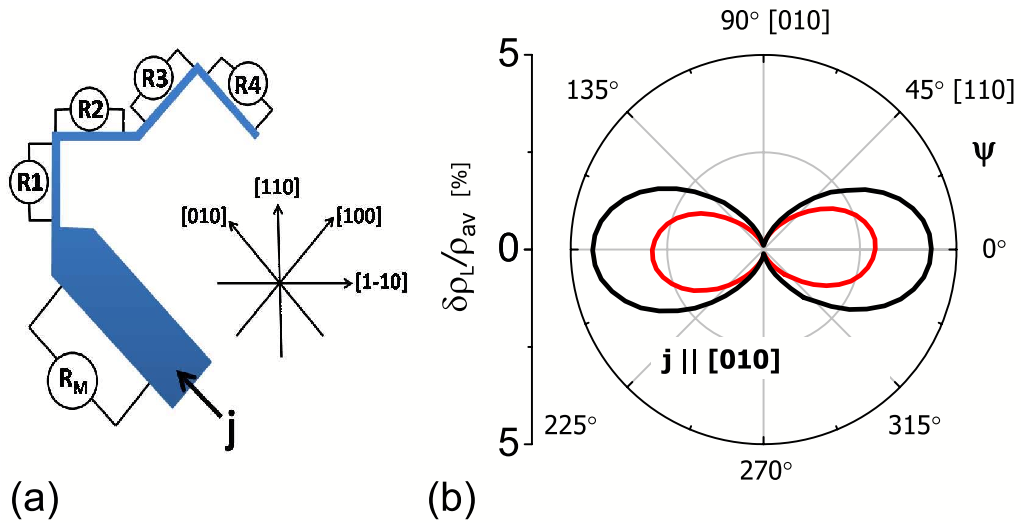
Figure 1. (a) Sketch of the first studied device with four microscopic bars in series together with a macroscopic Hall bar. Angular average of resistivity, ρ_{av}, at 4 T was 8.87, 14.7, 14.4 and 15 mΩ cm for the [110], [1$\bar{1}$0], [100] and [010] microbar and 18.3 mΩ cm for the [010] macrobar. (b) Polar plot of the percentage change in resistivity (AMR) as a function of the angle between the applied field of 4 T and the [100]-direction for the micro- and macroscopic bars aligned along the [010]-axis. Strain relaxation due to patterning leads to a reduction of the AMR magnitude of about 30%. For better clarity we plot, instead of $\Delta\rho_L/\rho_{av}$ defined in the section 2, $\delta\rho_L/\rho_{av} \equiv (\rho_L - \rho_{L,min})/\rho_{av}$. Here, $\rho_{L,min}$ is the minimum (with respect to ψ) longitudinal resistivity.

lithography and reactive ion etching in a 25 nm thick $Ga_{0.95}Mn_{0.05}As$ epilayer, which was grown along the [001] crystal axis on a GaAs substrate. The Curie temperature of the as-grown (Ga,Mn)As is 60 K. A compressive strain in the (Ga,Mn)As epilayer grown on the GaAs substrate leads to a strong magnetocrystalline anisotropy which forces the magnetization vector to align parallel with the plane of the magnetic epilayer [6, 7]. The growth strain is partly relaxed in the microbars, producing an additional, in-plane uniaxial tensile strain in the transverse direction [1]–[3].

Magnetoresistance traces were measured with the saturation magnetic field applied in the plane of the device, i.e. in the pure AMR geometry with zero (antisymmetric) Hall signal and with magnetization vector aligned with the external magnetic field. The sample was rotated by 360° with 5° steps. Longitudinal resistances of all five Hall-bars were measured simultaneously with lock-in amplifiers.

In figure 1(b), we show AMR data from magnetization rotation experiments in the 40 and 1 μm wide bars aligned along the [010]-direction. Both curves have a minimum for magnetization oriented parallel to the Hall bar axis and a maximum when magnetization is rotated by 90°. Although this is a typical characteristic of the non-crystalline AMR term in (Ga,Mn)As the large difference between the AMR magnitudes in the two devices points to a strong contribution of the crystalline AMR coefficient $C_U^{[010]}$ in equation (7), originating from the strain induced by transverse lattice relaxation in the microbar. We find that the magnitude of
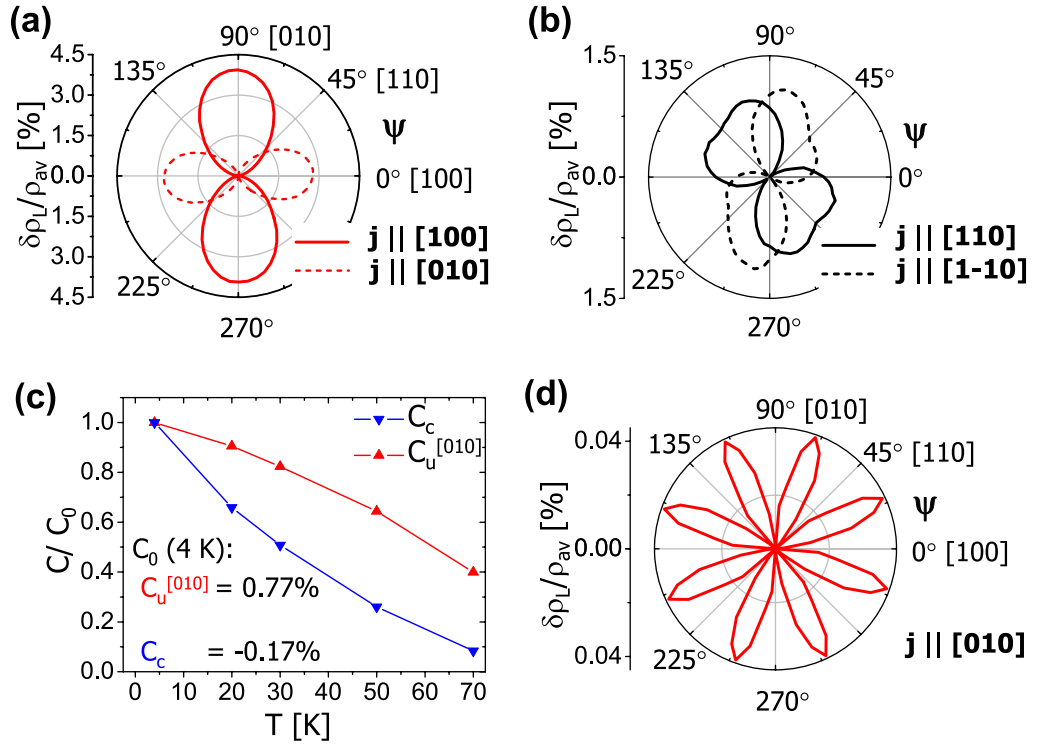
Figure 2. (a) and (b) AMR curves at $B = 4\,\mathrm{T}$ for the microscopic bars aligned along the in-plane cubic and diagonal directions, respectively. The magnitude of the AMR is about a factor of 3 smaller in the microbars along the diagonal directions. (c) Temperature dependence of the crystalline AMR coefficients normalized to the respective values C_0 at 4 K (shown in the inset). (d) Polar plot showing the eighth-order term found in the AMR of the microscopic bars, with a magnitude of 0.04%.

the coefficient, $C_U^{[010]} = 0.77$, amounts to about 30% of the magnitude of the total AMR in the unrelaxed macroscopic bar.

In figures 2(a) and (b), we plot AMR traces for microbars patterned along the [100]/[010] and [110]/[1$\bar{1}$0]-crystallographic directions. Strikingly, the overall magnitude of the AMR traces for the [110]/[1$\bar{1}$0]-oriented Hall bars is about a factor of 3 smaller than for the [100]/[010] bars and appears to have a much stronger relative contribution of the cubic crystalline term (the term proportional to C_C in equation (4)). However, by extracting the 90°-periodic AMR components for all microbars, as well as for the macroscopic Hall bar, we find a consistent value of $C_C = -0.17 \pm 0.01\%$. This implies that it is rather a suppression (enhancement) of the uniaxial AMR components for the [110]/[1$\bar{1}$0] ([100]/[010])-oriented bars which accounts for the difference in AMR traces in figures 2(a) and (b). Since $\theta = n \times 45°$ for the Hall bars studied in figures 1 and 2, and the lattice relaxation induced strains in these microbars are in the transverse direction, we can rewrite the ψ-dependent uniaxial terms for the longitudinal AMR in equations (6) and (7) in a compact form,

$$\Delta_L^{uni} = C_U^s \cos 2(\psi - \theta). \tag{8}$$

This expression, together with equation (4), implies that the amplitude of the total uniaxial (180°-periodic) contribution to the AMR in the [110]/[1$\bar{1}$0] devices ($|C_I + C_U^{[100]/[010]} + C_{IC}|$)

can indeed differ from that of the [100]/[010] devices ($|C_I + C_U^{[110]/[1\bar{1}0]} - C_{IC}|$), provided that C_{IC} is nonzero and/or $C_U^{[100]/[010]} \neq C_U^{[110]/[1\bar{1}0]}$.

Another observation we make is a broken [100]–[010] symmetry between the two AMR traces in figure 2(a) and in each of the two traces in figure 2(b). While in the former case this behavior can be captured by equation (8) taking $C_U^{[100]} \neq C_U^{[010]}$, the shape of the AMR curves in figure 2(b) is inconsistent with the form of equation (8). We have attempted to model the broken [100]–[010] symmetry by introducing a contribution to the $C_U^{[100]}$ coefficient which is independent of the microbar orientation, i.e. assuming that its origin is distinct from transverse strains induced by the micropatterning. From the difference between the two AMR curves in figure 2(a) and from the [1$\bar{1}$0]-bar AMR in figure 2(b), we obtained that this contribution is 0.3%, and from the [110]-bar AMR we obtained 0.1%. A bar-independent contribution to $C_U^{[100]}$ therefore explains only part of the observed [100]–[010] broken symmetry effects; we attribute the remaining part to possible material inhomogeneities or non-uniformities and misalignments in the micropatterning. It would be interesting to compare these conclusions also to ρ_T where the same anisotropy constants occur as in the ρ_L. The growth strain, however, cannot be relaxed at the contact leads, so that ρ_T will characterize mostly the unrelaxed portion of the Hall bar. On the other hand, the path at which ρ_L is measured, passes mostly through a relaxed region because the contact leads are very narrow compared to the longitudinal distance between the two contacts. The two quantities ρ_L and ρ_T thus characterize differently strained material in this case.

Importantly, the above experimental uncertainties have no effect on the main conclusion of our experiments that the lattice relaxation-induced uniaxial AMR coefficient is larger than the cubic crystalline component and a significant fraction of the total AMR of the unpatterned material. By normalizing the value of the transverse strain-induced $C_U^{[010]}$ coefficient and the C_C coefficient to the respective values at 4 K, we can also compare their temperature dependences within the measured range of temperatures of 4–70 K. Clearly, the C_C coefficient decreases more rapidly with increasing temperature. This recalls the behavior of the magnetocrystalline anisotropy terms in magnetization, where the uniaxial term decreases in a less pronounced way than the cubic one, since the former scales roughly with M^2, whereas the latter with M^4. As a result of this, the transverse strain-induced term becomes more dominant at higher temperatures, changing from 31% of the total AMR at 4 K, to 38% at 70 K (not shown)[6].

A detailed analysis of the longitudinal resistance measurements in the microbars allows us to identify higher-order cubic terms (see equation (A.4) in appendix A). By subtracting the second- and fourth-order terms from AMR data measured on the [010] microbar we find a clear signature of an eighth-order (45°-periodic) cubic term with an amplitude of 0.04%, as shown in figure 2(d). In section 4, we give another example of the unusual high-order AMR terms (and explain in more detail how these are extracted from the data) which emerge from post-growth-induced lattice distortion experiments.

Measurements in the Hall bars discussed above demonstrate that (sub)micrometre lithography of (Ga,Mn)As materials grown under lattice matching strains inevitably produces strain relaxation which may be large enough to significantly modify magnetotransport characteristics of the structure. Lateral micro and nanoconstrictions, utilized in magnetotransport studies of non-uniformly magnetized systems or as pinning centers for domain wall dynamics studies, are

---

[6] Note that nonzero AMR is still observable at 70 K which is above the T_c of the as-grown material. Possible reasons are the high-magnetic field (4 T) used and/or partial annealing during the device fabrication processes.
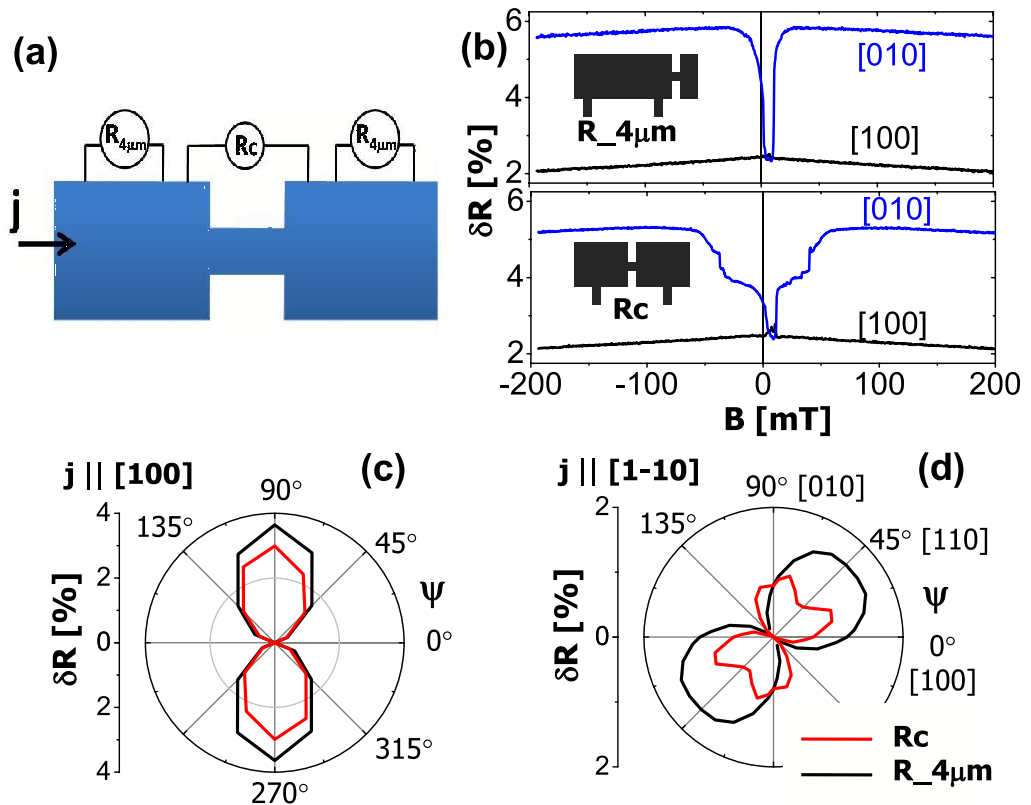
Figure 3. (a) Two devices consisting of a $4\,\mu m$ wide bar containing a $150\,nm$ wide and $500\,nm$ long constriction were patterned from the same wafer material as in figures 1 and 2: one device was oriented along the [100], another along the [1$\bar{1}$0]. (b) Resistance variations during in-plane magnetic field sweeps from negative to positive saturation fields applied along the [100] (black) and [010] (blue) directions, measured in the constriction device patterned along the [100]-crystallographic axis. Reference resistances $R = 13.7$ and $R_c = 22.0\,k\Omega$ correspond to $B = 4\,T$. (c,d) AMR measurements in the wider contact (black) and across the constriction (red) in a rotating saturation field of $4\,T$ for devices patterned along the [100]-direction (c) and along the [110]-direction (d). Angular averages of R/R_c are 13.5/21.6 (c), and 31.8/42.3 $k\Omega$ (d). Percentage change in resistances rather than resistivities are plotted for this non-uniform geometry device; the distinction is not relevant for the discussion of the relative changes in the longitudinal magnetoresistance.

an important class of devices for which these effects are highly relevant. In figure 3, we show data measured in devices consisting of two $4\,\mu m$ wide bars patterned from the same (Ga,Mn)As wafer as above along the [1$\bar{1}$0] (or [100])-crystallographic direction and connected by a $150\,nm$ wide and $500\,nm$ long constriction. Magnetic field sweep experiments at a fixed field angle, plotted in panel (b), illustrate a marked increase in the constriction of the anisotropy field along the [100]-bar direction at which magnetization rotates from saturation field orientations towards the easy [100]-axis. Because of the dilute moment nature of the (Ga,Mn)As ferromagnet, shape

IOP Institute of Physics ⏀ DEUTSCHE PHYSIKALISCHE GESELLSCHAFT

anisotropy plays only a minor role here and the effect is ascribed to strain relaxation and corresponding changes in the magnetocrystalline anisotropy in the constriction.

AMR measurements in a rotating $B = 4\,T$ field shown in figures 3(c) and (d) provide further indication of the presence of strong strain relaxation-induced magnetocrystalline effects in devices with narrow constrictions. The comparison between AMRs of the wider contacts and of the constriction shows very similar phenomenology to that of the macroscopic and strain-relaxed microscopic Hall bars discussed in the first part of this section (compare figure 2 and figures 3(c) and (d)). We again identify the uniaxial crystalline AMR term in the constriction due to microfabrication which is of the same sign and similar magnitude as observed in the micro Hall bars. Consistency is also found when comparing the character of the AMR curves for the micro Hall-bars and for the constriction devices patterned along the different crystallographic directions (see figures 2 and 3(c) and (d)).

4. Experiments in (Ga,Mn)As/piezo-transducer hybrid structures

Lithographic patterning of micro and nanostructures in (Ga,Mn)As provides powerful means for engineering the crystalline AMR components. In this section, we show that further electrical control of these effects is achieved in hybrid PZT/(Ga,Mn)As structures. A 25 nm thick $Ga_{0.94}Mn_{0.06}As$ epilayer utilized in the study was grown by low-temperature molecular-beam-epitaxy on GaAs substrate and buffer layers [4]. A macroscopic Hall bar, fabricated in the (Ga,Mn)As wafer by optical lithography, and orientated along the $[1\bar{1}0]$-direction, was bonded to the PZT using a two-component epoxy after thinning the substrate to $150 \pm 10\,\mu m$ by chemical etching. The stressor was slightly misaligned so that a positive/negative voltage produces a uniaxial tensile/compressive strain at $\approx -10°$ to the $[1\bar{1}0]$-direction. The induced strain was measured by strain gauges, aligned along the $[1\bar{1}0]$- and $[110]$-directions, mounted on a second piece of $150 \pm 10\,\mu m$ thick wafer bonded to the PZT. Differential thermal contraction of GaAs and PZT on cooling to 50 K produces a measured biaxial, in-plane tensile strain at zero bias of 10^{-3} and a uniaxial strain estimated to be of the order of $\sim 10^{-4}$ [27]. At 50 K, the magnitude of the additional strain for a PZT voltage of $\pm 150\,V$ is approximately 2×10^{-4}.

Previous measurements [4] of the device identified large changes in the magnetic easy axis orientation induced by the PZT. Here, we focus on the effects of the stressor on the magnetotransport coefficients. The AMR measured at 50 K for $\pm 150\,V$ on the transducer is shown in figure 4(a). The modification of the AMR induced by the strain can be extracted by subtracting curves at $\pm 150\,V$ (see figure 4(b)). It is expected that only the crystalline terms are modified; indeed the modification in the longitudinal resistivity ρ_L is due to the second- and fourth-order crystalline AMR terms. This is consistent with our previous analysis on the unstressed Hall bars, where we found that there were second- and fourth-order crystalline terms representing approximately 10% of the total AMR. There is also a modification of ρ_T of similar magnitude. This is predominantly due to the fourth-order term.

To extract the absolute value of the fourth-order term in ρ_T at each voltage we have performed the following analysis: starting with the raw ρ_T data we subtract any offset due to mixing of ρ_L into the ρ_T signal which may occur as a consequence of small inaccuracies in the Hall bar geometry or small inhomogeneity in the wafer. This is a correction of approx. 0.4% of the ρ_L signal which should have no significant effect on the subsequent analysis of fourth-order terms. (The fourth-order components in ρ_L are typically 0.1%, so the effect on ρ_T would be $0.4\% \times 0.1\% = 0.0004\%$, i.e. negligibly small.) We then remove any unintentional
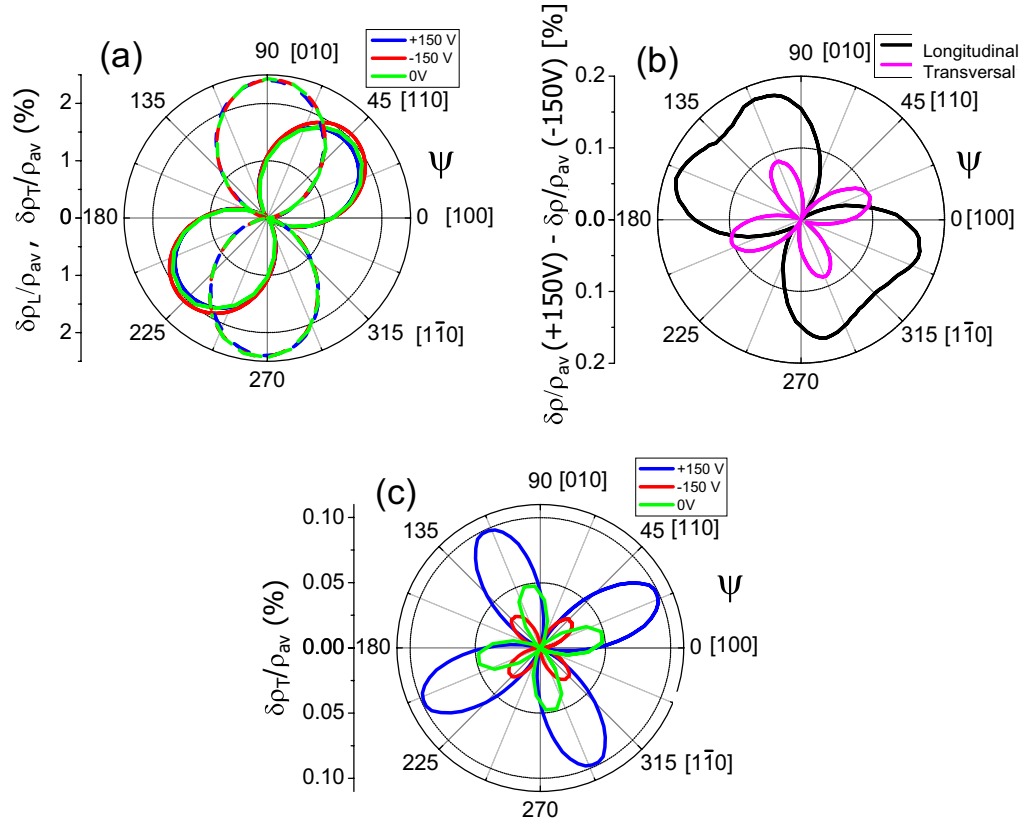
Figure 4. (a) The longitudinal (solid curves) and transverse (dashed curves) AMRs for piezo voltages $\pm150\,\text{V}$. (b) The differences between the longitudinal and transverse AMRs for piezo voltages $\pm150\,\text{V}$. (c) Fourth-order components of the transverse AMR at piezo voltages ±150 and $0\,\text{V}$ (second-order components were subtracted as described in the text). In all the cases, $T = 50\,\text{K}$ and the field of $1\,\text{T}$ was rotated in the plane of the (Ga,Mn)As layer. As in figures 1–3, we plot for better clarity $\delta\rho_{\text{L}}/\rho_{\text{av}} \equiv (\rho_{\text{L}} - \rho_{\text{L,min}})/\rho_{\text{av}}$ and $\delta\rho_{\text{T}}/\rho_{\text{av}} \equiv (\rho_{\text{T}} - \rho_{\text{T,min}})/\rho_{\text{av}}$ with $\rho_{\text{av}} \approx 5.3\,\text{m}\Omega\,\text{cm}$. Here $\rho_{\text{L(T),min}}$ is the minimum (with respect to ψ) longitudinal (transverse) resistivity.

antisymmetric (Hall) component from ρ_{T} by shifting the data by $180°$ and averaging. The second-order terms are subsequently removed from ρ_{T} by shifting the data by $90°$ and averaging. The result of this procedure is plotted in figure 4(c).

At the piezo voltage of $0\,\text{V}$ the fourth-order component is approximately 0.03% (peak to trough). At $+150\,\text{V}$ it is further enhanced to approximately 0.1% while at $-150\,\text{V}$ the magnitude is reduced to approximately 0.01% which is a value similar to the fourth-order term observed after carefully re-examining a (Ga,Mn)As wafer without the PZT attached to it [23]. For the present device, measurements of the magnetic anisotropy indicate that the application of $-150\,\text{V}$ to the PZT counteracts the uniaxial strain induced by differential thermal contraction on cooling to return the device close to the unstrained state [4]. The presence of a fourth-order term in the transverse AMR is allowed under a uniaxial distortion, see equations (A.8) and (7), but is not expected if only cubic symmetry is present. The positions of maxima

in figure 4(c) do not comply with equation (A.8) alone and they moreover change with the magnitude of the strain. We ascribe this observation to the PZT misalignment which implies that the actual strain has both a [110] and a [100] component. As the strain dependence of anisotropy constants like $C_{\mathrm{IU4+}}^{[110]}$ and $C_{\mathrm{IU4+}}^{[100]}$ may be different, shifts of maxima can occur. We also observed changes in the longitudinal AMR (not shown) which were comparable to those in the transverse AMR. Note that both in magnitude and in the position of maxima there may be differences between the longitudinal and transversal fourth-order components: while the latter depends on $-C_{\mathrm{IU4+}}^{[110]} + C_{\mathrm{IU4-}}^{[110]}$, see equation (A.8), the longitudinal AMR may change either via $C_{\mathrm{IU4+}}^{[110]} + C_{\mathrm{IU4-}}^{[110]}$ or via C_{C}, see equations (A.7) and (4).

The data presented in figure 4(c) clearly demonstrate that the uniaxial strain produced by the PZT induces a significant fourth-order term in the transverse AMR, which is usually considered to be of insignificant magnitude in the unstrained wafer. Note that the small misalignment of the magnetization with the 1 T applied field has a negligible effect here, as we checked by considering the magnetic anisotropy constants given in [4]. The analysis thus demonstrates that by applying voltage on the PZT one can significantly enhance crystalline AMR components, as compared to the bare (Ga,Mn)As wafer, and efficiently compensate additional strain effects induced by, e.g. different thermal expansion coefficients in hybrid multilayer structures.

5. Conclusions

We have demonstrated that besides the previously observed effects on magnetic anisotropies, post-growth strain engineering can be also used to manipulate efficiently the AMR of (Ga,Mn)As. Since magnetic anisotropy is a property of the total energy of the system while AMR also reflects quasiparticle scattering rate characteristics [23] there is no straightforward link between the two observations. Experiments and phenomenological analysis of the data have been presented for two distinct approaches to post-growth strain control: we used the transverse in-plane relaxation of the GaAs/(Ga,Mn)As lattice mismatch strain in lithographically patterned narrow Hall bars, and an electrically controlled strain was induced using a piezo-transducer. Our main results include the observation of AMR changes due to strain which can be comparable in magnitude to the strongest, non-crystalline AMR component in bare (Ga,Mn)As, and we have also reported previously undetected high-order crystalline AMR terms. Finally, we have demonstrated that strain-induced effects can play an important role in magnetoresistance characteristics of (Ga,Mn)As nanoconstrictions.

Acknowledgments

Note added in proof. While this article was under review, a report by Limmer *et al* [30] appeared on the arXiv presenting an extensive collection of AMR measurements in materials grown under various tensile and compressive strains.

Appendix A. Derivation of phenomenological AMR expressions

To derive the appropriate AMR expansions for cubic and uniaxially distorted crystals, we consider the conductivity tensor in equation (1) with the two Hall bars and magnetization vector fixed in space and perform the relevant symmetry operations to the underlying crystal. (Note that the values of ψ and θ may change under the effect of the symmetry operations since the angles are defined with respect to the crystallographic directions.) The relevant operations for the cubic crystal are summarized in table A.1; the last operation, the invariance under $\psi \to 90° - \psi$ assuming the Hall bars and the crystal fixed, is derived from the microscopic theoretical expression for the AMR [14]. The general form of equation (1) constrained by these cubic symmetry considerations reads:

$$\hat{\rho} = \hat{\rho}_{\text{cub}} = \begin{pmatrix} u(\cos^2 \psi) & \cos \psi \sin \psi \frac{v(\cos^2 \psi)+v(\sin^2 \psi)}{2} \\ \cos \psi \sin \psi \frac{v(\sin^2 \psi)+v(\cos^2 \psi)}{2} & u(\sin^2 \psi) \end{pmatrix}. \tag{A.1}$$

Functions u and v can be expanded in the Taylor series of $\cos^n \psi$ [25] or, equivalently, in the series of $\cos n\psi$. For example, for u in equation (A.1) we obtain,

$$u(\cos^2 \psi) = a_0 + a_2 \cos 2\psi + a_4 \cos 4\psi + \cdots \tag{A.2}$$

and

$$u(\sin^2 \psi) = a_0 - a_2 \cos 2\psi + a_4 \cos 4\psi - \cdots. \tag{A.3}$$

Equations (A.1)–(A.3) together with equation (2) yield, after transforming all products of goniometric functions and recollecting them into sines and cosines of sums of angles, the following structure of the longitudinal and transverse AMR expressions:

$$\frac{\Delta\rho_{\text{L}}}{\rho_{\text{av}}} = C_{\text{C}} \cos 4\psi + C_{\text{C8}} \cos 8\psi + \cdots$$
$$+ C_{\text{I}} \cos(2\psi - 2\theta) + C_{\text{IC}} \cos(2\psi + 2\theta)$$
$$+ C_{\text{I6}} \cos(6\psi - 2\theta) + C_{\text{IC6}} \cos(6\psi + 2\theta) + \cdots \tag{A.4}$$

and

$$\frac{\rho_{\text{T}}}{\rho_{\text{av}}} = + C_{\text{I}} \sin(2\psi - 2\theta) - C_{\text{IC}} \sin(2\psi + 2\theta)$$
$$+ C_{\text{I6}} \sin(6\psi - 2\theta) - C_{\text{IC6}} \sin(6\psi + 2\theta) + \cdots. \tag{A.5}$$

Equations (4) and (5) in section 2 are obtained by keeping all terms in (A.4) and (A.5) up to 4ψ. Note that there is a simple relationship between the longitudinal and transverse AMRs, $\rho_{\text{T}}/\rho_{\text{av}} = \frac{1}{2}(\partial(\Delta\rho_{\text{L}}/\rho_{\text{av}})/\partial\theta)$, which is a consequence of the symmetry $(\hat{\rho})_{ij} = (\hat{\rho})_{ji}$ in equation (A.1).

Analogous procedure can be applied to cubic crystals with uniaxial strain along the [110]-direction; corresponding symmetry operations are listed in table A.2 and $\hat{\rho}$ in this case reads,

$$\hat{\rho} = \hat{\rho}_{\text{cub}} + \begin{pmatrix} t(\cos^2 \psi) \cos \psi \sin \psi & \frac{1}{2}[w(\cos^2 \psi) + w(\sin^2 \psi)] \\ \frac{1}{2}[w(\cos^2 \psi) + w(\sin^2 \psi)] & t(\sin^2 \psi) \cos \psi \sin \psi \end{pmatrix}. \tag{A.6}$$

Table A.1. Symmetry operations used for a cubic crystal.

Symmetry operation	Implied conditions on $\hat{\rho}$
Symmetry along [010]	$\rho_{11}(\cos\psi, \sin\psi) = \rho_{11}(-\cos\psi, \sin\psi)$
Symmetry along [110]	$\rho_{11}(\cos\psi, \sin\psi) = \rho_{22}(\sin\psi, \cos\psi)$
	$\rho_{12}(\cos\psi, \sin\psi) = \rho_{21}(\sin\psi, \cos\psi)$
Symmetry along [1$\bar{1}$0]	$\rho_{11}(\cos\psi, \sin\psi) = \rho_{22}(-\sin\psi, -\cos\psi)$
Rotation by 90°	$\rho_{12}(\cos\psi, \sin\psi) = -\rho_{21}(-\sin\psi, \cos\psi)$
Invariance under $\psi \to 90° - \psi$ (fixed crystal)	$\rho_{12}(\cos\psi, \sin\psi) = \rho_{12}(\sin\psi, \cos\psi)$

Table A.2. Symmetry operations used for cubic crystal uniaxially strained along [110].

Symmetry operation	Implied conditions on $\hat{\rho}$
Symmetry along [110]	$\rho_{11}(\cos\psi, \sin\psi) = \rho_{22}(\sin\psi, \cos\psi)$
	$\rho_{12}(\cos\psi, \sin\psi) = \rho_{21}(\sin\psi, \cos\psi)$
Symmetry along [1$\bar{1}$0]	$\rho_{11}(\cos\psi, \sin\psi) = \rho_{22}(-\sin\psi, -\cos\psi)$
	$\rho_{12}(\cos\psi, \sin\psi) = \rho_{21}(-\sin\psi, -\cos\psi)$
Invariance under $\psi \to 90° - \psi$ (fixed crystal)	$\rho_{12}(\cos\psi, \sin\psi) = \rho_{12}(\sin\psi, \cos\psi)$

Equation (A.6) yields the following uniaxial AMR terms:

$$
\begin{aligned}
\frac{\Delta\rho_L}{\rho_{av}} = & \, C_U^{[110]} \sin 2\psi + C_{U6}^{[110]} \sin 6\psi + C_{U10}^{[110]} \sin 10\psi + \cdots \\
& + C_{IU}^{[110]} \sin 2\theta + C_{IU4+}^{[110]} \sin(4\psi - 2\theta) \\
& + C_{IU4-}^{[110]} \sin(4\psi + 2\theta) + C_{IU8+}^{[110]} \sin(8\psi - 2\theta) \\
& + C_{IU8-}^{[110]} \sin(8\psi + 2\theta) + \cdots
\end{aligned}
\tag{A.7}
$$

and

$$
\begin{aligned}
\frac{\rho_T}{\rho_{av}} = & + C_{IU}^{[110]} \cos 2\theta - C_{IU4+}^{[110]} \cos(4\psi - 2\theta) \\
& + C_{IU4-}^{[110]} \cos(4\psi + 2\theta) - C_{IU8+}^{[110]} \cos(8\psi - 2\theta) \\
& + C_{IU8-}^{[110]} \cos(8\psi + 2\theta) + \cdots .
\end{aligned}
\tag{A.8}
$$

The terms which contain at most 2ψ reproduce equation (6).

Cubic crystals with uniaxial strain along the [100]-axis are described by (see table A.3),

$$
\hat{\rho} = \begin{pmatrix} u(\cos^2\psi) + \Delta u(\cos^2\psi) & \sin\psi\cos\psi[v(\cos^2\psi) + \Delta v(\cos^2\psi)] \\ \sin\psi\cos\psi[v(\sin^2\psi) - \Delta v(\sin^2\psi)] & u(\sin^2\psi) - \Delta u(\sin^2\psi) \end{pmatrix} . \tag{A.9}
$$

Table A.3. Symmetry operations used for a cubic crystal uniaxially strained along [100].

Symmetry operation	Implied conditions on $\hat{\rho}$
Symmetry along [100]	$\rho_{11}(\cos\psi, \sin\psi) = \rho_{11}(\cos\psi, -\sin\psi)$
	$\rho_{22}(\cos\psi, \sin\psi) = \rho_{22}(\cos\psi, -\sin\psi)$
	$\rho_{12}(\cos\psi, \sin\psi) = -\rho_{12}(\cos\psi, -\sin\psi)$
	$\rho_{21}(\cos\psi, \sin\psi) = -\rho_{21}(\cos\psi, -\sin\psi)$
Symmetry along [010]	$\rho_{11}(\cos\psi, \sin\psi) = \rho_{11}(-\cos\psi, \sin\psi)$
	$\rho_{22}(\cos\psi, \sin\psi) = \rho_{22}(-\cos\psi, \sin\psi)$
	$\rho_{12}(\cos\psi, \sin\psi) = -\rho_{12}(-\cos\psi, \sin\psi)$
	$\rho_{21}(\cos\psi, \sin\psi) = -\rho_{21}(-\cos\psi, \sin\psi)$

Note that $(\hat{\rho})_{ij} \neq (\hat{\rho})_{ji}$ in this case. Equation (A.9) yields the following uniaxial AMR terms:

$$
\begin{aligned}
\frac{\Delta\rho_{\mathrm{L}}}{\rho_{\mathrm{av}}} = {} & C_{\mathrm{U}}^{[100]}\cos 2\psi + C_{\mathrm{U6}}^{[100]}\cos 6\psi + C_{\mathrm{U10}}^{[100]}\cos 10\psi + \cdots \\
& + C_{\mathrm{IU}}^{[100]}\cos 2\theta + C_{\mathrm{IU4+}}^{[100]}\cos(4\psi - 2\theta) \\
& + C_{\mathrm{IU4-}}^{[100]}\cos(4\psi + 2\theta) + C_{\mathrm{IU8+}}^{[100]}\cos(8\psi - 2\theta) \\
& + C_{\mathrm{IU8-}}^{[100]}\cos(8\psi + 2\theta) + \cdots,
\end{aligned}
\tag{A.10}
$$

and

$$
\begin{aligned}
\frac{\rho_{\mathrm{T}}}{\rho_{\mathrm{av}}} = {} & + C_{\mathrm{U,T}}^{[100]}\sin 2\psi + C_{\mathrm{U4,T}}^{[100]}\sin 4\psi + C_{\mathrm{U6,T}}^{[100]}\sin 6\psi + \cdots \\
& - C_{\mathrm{IU}}^{[100]}\sin 2\theta + C_{\mathrm{IU4+}}^{[100]}\sin(4\psi - 2\theta) \\
& - C_{\mathrm{IU4-}}^{[100]}\sin(4\psi + 2\theta) + C_{\mathrm{IU8+}}^{[100]}\sin(8\psi - 2\theta) \\
& - C_{\mathrm{IU8-}}^{[100]}\sin(8\psi + 2\theta) + \cdots.
\end{aligned}
\tag{A.11}
$$

Again, the lowest order terms reproduce equation (7).

Appendix B. Definitions of transport anisotropy constants

The first impression one probably gets from researching the literature on AMR is that every publication uses its own definition of anisotropy constants. This is naturally not completely true, nevertheless, linking results between different publications indeed requires some effort. All works mentioned below, including the present one, are based or expand either on the analysis of Döring [25] or Birss [28].

Generally, the resistivity tensor of equation (1) should be a 3×3 matrix and this introduces, compared to results in appendix A, new anisotropy constants and also a second angle determining the direction of magnetization. If this is the starting point, expressions for AMR on an arbitrarily oriented surface can be derived. In our work, we focused on (001) surfaces, and

obtained simple formulae, as for instance equations (4) and (5), however, at the cost of some loss of generality. In simple terms, not all constants which appear in literature in expansions of the 3×3 resistivity tensor can be recovered.

1. The most common symbols are $\rho_\parallel$ and $\rho_\perp$, the resistivities for magnetization-oriented parallel and perpendicular to current (used e.g. in [17, 20]). It holds

$$C_{\mathrm{I}} = \frac{\rho_\parallel - \rho_\perp}{\rho_\parallel + \rho_\perp},$$

   for polycrystalline (or isotropic) system, where this single constant fully describes all possible anisotropies (cf equation (3)). We point out that apparently different values of $\rho_\parallel - \rho_\perp$ derived from the longitudinal and transverse resistivities as the coefficient in front of the 180°-periodic component in [17], are just a simple consequence of lowering the isotropic symmetry: they correspond to $C_{\mathrm{I,C}} \neq 0$ as can be seen in equations (4) and (5).

2. Limmer *et al* [16] derive the most general form of the 3×3 resistivity tensor up to terms quadratic in direction cosines of the magnetization, i.e. $\cos^2 \psi$ in the case of (001) surfaces and equation (1). They consider a cubic crystal with a tetragonal lattice distortion along [001], aiming at a description of (Ga,Mn)As layers subject to strain due to the lattice mismatch with the substrate. The link between constants A, B, C, and D defined in equation (3) of [16] (pure cubic system) and our equations (4) and (5) is

$$C_{\mathrm{I}} = \frac{B + C}{4A}, \quad C_{\mathrm{I,C}} = \frac{B - C}{4A}.$$

   The constant D is completely decoupled from AMR within (001) layers.

   The uniaxial strain discussed in our work is different from the tetragonal lattice distortion considered in [16]. However, $C_{\mathrm{U}}^{[100]}$ in our equation (7) corresponds to $2b_1/A$ in equation (A.8) of [16] if $b_1 = b_2$ and axes [100] and [001] are interchanged.

3. McGuire and Potter [26] give expansions of the 3×3 resistivity tensor for cubic system up to the fourth power of magnetization direction cosines. Their constants C_0' through C_5' map to equations (4) and (5) in the following way:

$$C_{\mathrm{I}} = \frac{C_1' + C_4' + C_2'}{4C_0'}, \quad C_{\mathrm{I,C}} = \frac{C_1' - C_4' + C_2'}{4C_0'}, \quad C_{\mathrm{C}} = \frac{C_2'}{8C_0'}.$$

   Again, C_3' and C_5' cannot be determined from AMR in (001) layers.

4. Döring [25] performs an analysis equivalent to the later work of McGuire and Potter [26] but using slightly different constants k_1 through k_5. The relationship to equations (4) and (5) is

$$C_{\mathrm{I}} = \frac{k_1 + k_2 + k_4}{4}, \quad C_{\mathrm{I,C}} = \frac{k_1 - k_2 + k_4}{4}, \quad C_{\mathrm{C}} = \frac{k_4 - 3k_3}{24}.$$

   The main results of this work are reviewed by van Gorkom *et al* [29] who study epitaxial iron films and use the same definition of transport anisotropy constants.

   Finally, we point out that all symmetry analyses, the present one and those referenced above, start with writing the AMR as a polynomial in direction cosines of the magnetization and of the current. It is, however, reasonable to re-express such formulae in terms of cosines of multiples of an angle at the end because the natural way of analyzing both experimental

and microscopically calculated data is to split the AMR into its Fourier components, e.g. as suggested by equation (4). The functional spaces spanned by $B_1 = \{1, \cos^2 \psi, \cos^4 \psi, \ldots\}$ and $B_2 = \{1, \cos 2\psi, \cos 4\psi, \ldots\}$ are of course identical, but the recalculation of coefficients of some particular AMR data with respect to the basis B_2 to coefficients with respect to the *non-orthogonal* basis B_1 depends on how many elements we keep in the basis. In other words, if we at some point decide to study higher order terms such as $\cos 8\psi$ shown in figure 2(d) and define the AMR coefficients with respect to the basis B_1, then also the coefficients in front of the 'old' terms 1, $\cos^2 \psi$ and $\cos^4 \psi$ have to be recalculated. We therefore prefer the definition used in equation (4).

References

[1] Hümpfner S, Sawicki M, Pappert K, Wenisch J, Brunner K, Gould C, Schmidt G, Dietl T and Molenkamp L W 2007 Lithographic engineering of anisotropies in (Ga,Mn)As *Appl. Phys. Lett.* **90** 102102

[2] Wunderlich J *et al* 2007 Local control of magnetocrystalline anisotropy in (Ga,Mn)As microdevices: demonstration in current-induced switching *Phys. Rev.* B **76** 054424

[3] Wenisch J, Gould C, Ebel L, Storz J, Pappert K, Schmidt M J, Kumpf C, Schmidt G, Brunner K and Molenkamp L W 2007 Control of magnetic anisotropy in (Ga,Mn)As by lithography-induced strain relaxation *Phys. Rev. Lett.* **99** 077201

[4] Rushforth A W *et al* 2008 Voltage control of magnetocrystalline anisotropy in ferromagnetic–semiconductor/piezoelectric hybrid structures *Preprint* 0801.0886

[5] Overby M, Chernyshov A, Rokhinson L P, Liu X and Furdyna J K 2008 GaMnAs-based hybrid multiferroic memory device *Preprint* 0801.4191

[6] Dietl T, Ohno H and Matsukura F 2001 Hole-mediated ferromagnetism in tetrahedrally coordinated semiconductors *Phys. Rev.* B **63** 195205

[7] Abolfath M, Jungwirth T, Brum J and MacDonald A H 2001 Theory of magnetic anisotropy in III$_{1-x}$Mn$_x$V ferromagnets *Phys. Rev.* B **63** 054418

[8] Goennenwein S T B, Althammer M, Bihler C, Brandlmaier A, Geprägs S, Opel M, Schoch W, Limmer W, Gross R and Brandt M S 2008 Piezo-voltage control of magnetization orientation in a ferromagnetic semiconductor *Phys. Status Solidi (RRL)* **2** 96

[9] Kim S-K, Lee J-W, Shin S-C, Song H W, Lee C H and No K 2003 Voltage control of a magnetization easy axis in piezoelectric/ferromagnetic hybrid films *J. Magn. Magn. Mater.* **267** 127

[10] Lee J-W, Shin S-C and Kim S-K 2003 Spin engineering of CoPd alloy films via the inverse piezoelectric effect *Appl. Phys. Lett.* **82** 2458

[11] Botters B, Giesen F, Podbielski J, Bach P, Schmidt G, Molenkamp L W and Grundler D 2006 Stress dependence of ferromagnetic resonance and magnetic anisotropy in a thin NiMnSb film on InP(001) *Appl. Phys. Lett.* **89** 242505

[12] Boukari H, Cavaco C, Eyckmans W, Lagae L and Borghs G 2007 Voltage assisted magnetic switching in Co$_{50}$Fe$_{50}$ interdigitated electrodes on piezoelectric substrates *J. Appl. Phys.* **101** 054903

[13] Jungwirth T, Sinova J, Wang K Y, Edmonds K W, Campion R P, Gallagher B L, Foxon C T, Niu Q and MacDonald A H 2003 Dc-transport properties of ferromagnetic (Ga,Mn)As semiconductors *Appl. Phys. Lett.* **83** 320

[14] Jungwirth T, Abolfath M, Sinova J, Kučera J and MacDonald A H 2002 Boltzmann theory of engineered anisotropic magnetoresistance in (Ga,Mn)As *Appl. Phys. Lett.* **81** 4029

[15] Matsukura F, Sawicki M, Dietl T, Chiba D and Ohno H 2004 Magnetotransport properties of metallic (Ga,Mn)As films with compressive and tensile strain *Physica* E **21** 1032

IOP Institute of Physics Φ DEUTSCHE PHYSIKALISCHE GESELLSCHAFT

[16] Limmer W, Glunk M, Daeubler J, Hummel T, Schoch W, Sauer R, Bihler C, Huebl H, Brandt M S and Goennenwein S T B 2006 Angle-dependent magnetotransport in cubic and tetragonal ferromagnets: application to (001)- and (113)a-oriented (Ga,Mn)As *Phys. Rev.* B **74** 205205

[17] Muduli P K, Friedland K J, Herfort J, Schönherr H P and Ploog K H 2005 Antisymmetric contribution to the planar Hall effect of Fe_3Si films grown on GaAs(113)a substrates *Phys. Rev.* B **72** 104430

[18] Goennenwein S T B, Keizer R S, Schink S W, van Dijk I, Klapwijk T M, Miao G X, Xiao G and Gupta A 2007 Planar Hall effect and magnetic anisotropy in epitaxially strained chromium dioxide thin films *Appl. Phys. Lett.* **90** 142509

[19] Baxter D V, Ruzmetov D, Scherschligt J, Sasaki Y, Liu X, Furdyna J K and Mielke C H 2002 Anisotropic magnetoresistance in $Ga_{1-x}Mn_xAs$ *Phys. Rev.* B **65** 212407

[20] Tang H X, Kawakami R K, Awschalom D D and Roukes M L 2003 Giant planar Hall effect in epitaxial (Ga,Mn)As devices *Phys. Rev. Lett.* **90** 107201

[21] Goennenwein S T B, Russo S, Morpurgo A F, Klapwijk T M, Van Roy W and De Boeck J 2005 Quantitative study of magnetotransport through a (Ga,Mn)As single ferromagnetic domain *Phys. Rev.* B **71** 193306

[22] Wang K Y, Edmonds K W, Campion R P, Zhao L X, Foxon C T and Gallagher B L 2005 Anisotropic magnetoresistance and magnetic anisotropy in high-quality (Ga,Mn)As films *Phys. Rev.* B **72** 085201

[23] Rushforth A W *et al* 2007 Anisotropic magnetoresistance components in (Ga,Mn)As *Phys. Rev. Lett.* **99** 147207

[24] Rushforth A W *et al* 2007 The origin and control of the sources of AMR in (Ga,Mn)As devices *Preprint* 0712.2581

[25] Döring W 1938 Die Abhängigkeit des widerstandes von nickelkristallen von der richtung der spontanen magnetisierung *Ann. Phys., Lpz.* **424** 259

[26] McGuire T and Potter R 1975 Anisotropic magnetoresistance in ferromagnetic 3d alloys *IEEE Trans. Magn.* **11** 1018

[27] Habib B, Shabani J, De Poortere E P, Shayegan M and Winkler R 2007 Anisotropic low-temperature piezoresistance in (311)a GaAs two-dimensional holes *Appl. Phys. Lett.* **91** 012107

[28] Birss R R 1964 *Symmetry and Magnetism* (North-Holland: Amsterdam)

[29] van Gorkom R P, Caro J, Klapwijk T M and Radelaar S 2001 Temperature and angular dependence of the anisotropic magnetoresistance in epitaxial Fe films *Phys. Rev.* B **63** 134432

[30] Limmer W, Daeubler J, Dreher L, Glunk M, Schoch W, Schwaiger S and Sauer R 2008 Advanced resistivity model for arbitrary magnetization orientation applied to a series of compressive- to tensile-strained (Ga,Mn)As layers *Preprint* 0802.2635